Research, Society and Development, v. 11, n. 2, e3811225373, 2022
(CC BY 4.0) | ISSN 2525-3409 | DOI: http://dx.doi.org/10.33448/rsd-v11i2.25373

Synthesis, characterization, and photocatalytic activity of ZnO nanostructures

Síntese, caracterização e atividade fotocatalítica de nanoestruturas de ZnO

Síntesis, caracterización y actividad fotocatalítica de nanoestructuras de ZnO

Received: 01/05/2022 | Reviewed: 01/11/2022 | Accept: 01/15/2022 | Published: 01/17/2022

Maria Laura Della Costa Silveira
ORCID: https://orcid.org/0000-0002-3426-5571
São Paulo State University, Brazil
E-mail: maria.laura@unesp.br
Nathalia Rodrigues da Silva
ORCID: https://orcid.org/0000-0001-7392-4106
São Paulo State University, Brazil
E-mail: nathalia.r.silva@unesp.br
David Santos Souza Padovini
ORCID: https://orcid.org/0000-0003-4231-8802
São Paulo State University, Brazil
E-mail: nathalia.r.silva@unesp.br
Angela Kinoshita
ORCID: https://orcid.org/0000-0002-5057-1667
University of Western São Paulo, Brazil
E-mail: angelamitie@gmail.com
Fenelon Martinho Lima Pontes
ORCID: https://orcid.org/0000-0001-6086-5303
São Paulo State University, Brazil
E-mail: fm.pontes@unesp.br
Aroldo Geraldo Magdalena
ORCID: https://orcid.org/0000-0003-3385-2106
São Paulo State University, Brazil
E-mail: Aroldo.magdalena@unesp.br

Abstract
This study investigated the synthesis, characterization of ZnO nanostructures using different precipitating agents in the photodegradation of rhodamine B (Rh B) using scanning electron microscopy (SEM), X-ray diffraction (XRD), fourier transform infrared (FTIR) and UV/Vis spectroscopy and zeta potential measurements. The results indicated the dependence of morphology on calcination temperature and the precipitating agent. The colloidal stability of these nanomaterials is affected with the morphology changed. The photocatalytic results showed that ZnO nanostructures synthesized with NH_4OH (98.98%) were more efficient in the degradation of Rh B than ZnO nanostructures synthesized with NaOH (62.68%). This is related to ZnO (NH_4OH) nanoparticles should present a higher density of electronic defects than ZnO (NaOH), producing energy levels between the band gaps. These results are potentially associated with a combination of optical and geometric factors that create other paths for the generation of electron-hole pairs in the precipitated ZnO nanocatalyst with different alkaline solutions.
Keywords: Nanostructure; ZnO; Photodegradation; Rhodamine B.

Resumo
Neste trabalho estudou-se a síntese, caracterização de nanoestruturas de ZnO utilizando diferentes agentes precipitantes na fotodegradação de rodamina B (Rh B) utilizando microscopia eletrônica de varredura (MEV), difração de raios X (DRX), espectroscopia de infravermelho por transformada de Fourier (FTIR) e de UV/Vis e medidas de potencial zeta. Os resultados indicaram a dependência da morfologia da temperatura de calcinação e do agente precipitante. A estabilidade coloidal desses nanomateriais foi afetada com a alteração da morfologia. Os resultados fotocatalíticos mostraram que as nanoestruturas de ZnO sintetizadas com NH_4OH (98,98%) foram mais eficientes na degradação de Rh B do que as nanoestruturas de ZnO sintetizadas com NaOH (62,68%). Isso está relacionado ao fato de que nanopartículas de ZnO (NH_4OH) deveriam apresentar maior densidade de defeitos eletrônicos do que ZnO (NaOH), produzindo níveis de energia entre os band gaps. Esses resultados estão potencialmente associados a uma combinação de fatores ópticos e geométricos que criam outros caminhos para a geração de pares elétron-buraco no nanocatalisador de ZnO precipitado com diferentes soluções alcalinas.
Palavras-chave: Nanoestruturas; ZnO; Fotodegradação; Rodamina B.

Resumen
En este trabajo se estudió la síntesis, caracterización de nanoestructuras de ZnO utilizando diferentes agentes precipitantes en la fotodegradación de rodamina B (Rh B) mediante microscopía electrónica de barrido (SEM), difracción de rayos X (XRD), espectroscopía infrarroja por transformada de Fourier (FTIR) y y UV / Vis, y mediciones de potencial zeta. Los resultados indicaron la dependencia de la morfología de la temperatura de calcinación y el agente precipitante. La estabilidad coloidal de estos nanomateriales se vio afectada por el cambio de morfología. Los resultados fotocatalíticos mostraron que las nanoestructuras de ZnO sintetizadas con NH_4OH (98,98%) fueron más eficientes en la degradación de Rh B que las nanoestructuras de ZnO sintetizadas con NaOH (62,68%). Esto está relacionado con el hecho de que las nanopartículas de ZnO (NH_4OH) deberían tener una mayor densidad de defectos electrónicos que el ZnO (NaOH), produciendo niveles de energía entre los espacios de banda. Estos resultados están potencialmente asociados con una combinación de factores ópticos y geométricos que crean otras vías para la generación de pares de agujeros de electrones en el nanocatalizador de ZnO precipitado con diferentes soluciones alcalinas.
Palabras clave: Nanoestructuras; ZnO; Fotodegradación; Rodamina B.

1. Introduction

There is a growing interest in ZnO nanostructures because this material is highly applicable to solar cells (Shi et al. 2013; Maia et al. 2016; Jiong et al. 2006; Ahmad et al. 2021), gas sensors (Wang et al. 2012), capacitor-varistors (Walia et al. 2012), electrochemical nanodevices (Shetti et al. 2019; Willander et al. 2009), environmental remediation (Kumar et al. 2018), cosmetics (Awan et al. 2018; Kuo et al. 2019), among others. The ZnO nanostructures have highly efficient optical properties related to photocatalytic activity in comparison to corresponding nanoparticles such as TiO_2. Gu et al. (2020) observed that ZnO nanoparticles are promising alternatives to TiO_2, considering their electronic properties have similar band gap values, potentials, absorption coefficients, and load transfer mobility. It is also discussed that, in comparison to anatase TiO_2, wurtzite ZnO nanoparticles present a higher absorption coefficient due to the band gap, promoting improved performance and higher efficiency in the photodegradation of organic dyes. Kouhail et al. (2020) performed studies analyzing the photodegradation performance of ZnO nanoparticles synthesized with the direct precipitation method and TiO_2 nanoparticles synthesized with the sol-gel method, both presenting a well-distributed and spherical morphology. The nanoparticles were assessed for the photodegradation of three commercial textile dyes by sunlight and the ZnO nanoparticles showed the highest degradation efficiency of the dyes tested.

Different synthesis methodologies to obtain ZnO provide a variety of morphologies such as nanoflowers, nanotubes, nanowires, nanorings, nanorods, among potential others (Arya et al. 2012; Salehi-Babarsad et al. 2019), representing material of controllable morphology upon synthetic conditions. The morphology of ZnO nanoparticles directly affects photocatalytic ability. Moreover, an important characteristic of ZnO semiconductors is the correlation between band gap and size of nanoparticles, allowing adjustments according to the study requirements. One of the most relevant environmental applications is using these nanoparticles in a metal adsorption process (Zeng at al. 2020; Noreen et al. 2020) or the photodegradation of organic compounds (Alvi et al. 2017; Wang et al. 2015). Thus, studies are required on the controlled synthesis of this material according to the type of application, such as the use as an anode in electrochemical processes or a catalytic semiconductor in photochemical activities. Differences in the catalytic behavior of ZnO nanoparticles are partially related to grain boundaries (Cao et al. 2017). Wang et al. (2015) performed studies with ZnO nanoparticles synthesized through the hydrothermal method, with changes in the synthetic route and achievement of different morphologies at 160°C. They established that small particles with high surface oxygen vacancy are the best catalysts for dye photodegradation, which the combination of structural and electrical effects confirmed the excellent photoactivity of the material. Among the five samples, degradation rates ranged from ~ 45 to 100% of Rh B dye removal at the concentration of 7 mg L^{-1}, under light irradiation of 250 W for 30 minutes. The study by Giraldi et al. (2016) showed that ZnO synthesized with the polymeric precursor method presented 75% of degradation of the methylene blue dye in 180 minutes, with a band gap of 3.1 eV. Cavalcante et al. (2019) used ZnO synthesized with the

Pechinie method and obtained 70% of degradation of the methylene blue dye in 140 minutes. Moreover, zinc oxide presents non-toxic characteristics, low cost, and high availability (Cao et al. 2017). New studies with temperature changes, precipitating agents in a simple and low-cost synthetic route become important to improve ZnO properties. Therefore, the present study investigated the synthesis of ZnO nanoparticles using NaOH and NH_4OH as precipitating agents, analyzing their direct action on the morphology and electronic properties. It also analyzed the influence of time and temperature of the heat treatment, establishing its application as a catalyst in the photodegradation of Rhodamine B dye.

2. Methodology

The materials used in this study were 97.0% zinc chloride, $ZnCl_2$ (Sigma-Aldrich); 97.0% sodium hydroxide, NaOH (Dynamic); 25-28% ammonium hydroxide, NH_4OH (Synth); 99.5% ethanol (Synth), Rhodamine B dye (Synth).

2.1 Synthesis of ZnO nanoparticles

The ZnO nanoparticles were synthesized with the co-precipitation method (Lanje et al. 2013). Initially, 200 mL of 0.05 mol L^{-1} $ZnCl_2$ solution was prepared. Two base solutions were used as the precipitating agent (NaOH and NH_4OH). The first sample used 100 mL of 0.20 mol L^{-1} NaOH solution and the second sample used 5.00 mL of concentrated NH_4OH solution. The base solutions (NaOH and NH_4OH) were added to the $ZnCl_2$ solution, with the formation of $Zn(OH)_2$, as presented in reactions (I) and (II), respectively.

$$ZnCl_{2(aq)} + 2\ NaOH_{(aq)} \rightarrow Zn(OH)_{2(s)} + 2\ Na^{+}_{(aq)} + 2\ Cl^{-}_{(aq)} \quad (I)$$

$$ZnCl_{2(aq)} + 2\ NH_4OH_{(aq)} \rightarrow Zn(OH)_{2(s)} + 2\ NH_4{}^{+}_{(aq)} + 2\ Cl^{-}_{(aq)} \quad (II)$$

The reaction occurred under vigorous stirring for 2 hours at room temperature. Then, this solution remained at rest for 24 hours. Subsequently, the precipitate was separated and washed abundantly with water and ethanol until reaching a pH of 7.0. Finally, the precipitates obtained were dried at 80°C in an oven and subsequently calcinated at 100 and 200°C. After the heat treatments the formation of ZnO occurs. The calcination time varied from 1 to 4 hours at indicated temperatures.

2.2 Photocatalysis experiments

The photocatalytic activity for ZnO samples was evaluated by monitoring the photodegradation of Rhodamine B dye from an aqueous solution (indicated as Rh B) under UV (Philips 26 W lamp) as a light source at 25 ± 2°C. The photochemical reactor was made of a Pyrex glass jacketed quartz tube (photoreactor vessel, 30 mL). The photocatalytic reaction was performed as follows: 50 mg of the photocatalyst was added to 10 mL of Rh B aqueous solution (10 ppm). Before irradiation, the suspension was sonicated for 10 min and magnetically stirred in the dark for 10 min to obtain an adsorption equilibrium with the photocatalyst. Finally, the solution was exposed to the irradiation of a Philips 26 W lamp. Periodically during irradiation, 5,0 mL aliquots of the reaction solution were withdrawn from the photoreactor vessel and centrifuged to remove the catalyst. The supernatant solution was then loaded in a quartz cell (1 mL) with a 10-mm optical path to measure the variation of Rh B concentration by recording the corresponding absorbance peak at 554 nm. The optical absorption spectra were recorded on a UV-Vis spectra Varian Cary 5000 spectrophotometer at room temperature.

2.3 Characterization

The crystal structures were investigated by X-ray diffraction (XRD) recorded by a Rigaku miniflex 600 using Cu Kα radiation with a 2θ scanning step of 0.04º. Sample morphology was analyzed with a field emission scanning electron microscope (FESEM, FEI Inspect F50), which was operated at an accelerating voltage of 5 kV. The UV-Vis spectra were collected on a Varian Cary 5000 spectrophotometer by diffuse reflectance within the 800-200 nm range. The Zetasizer Nano ZS system equipment (Malvern Instruments) was used to measure zeta potential. The pH variations were controlled with 0.1 mol L^{-1} HCl or NaOH in 0.001 mol L^{-1} NaCl solution.

3. Results and Discussion

The XRD pattern was used to investigate the crystallinity of the ZnO final products. Figure 1 shows the XRD patterns of ZnO nanostructures, which were precipitated with NaOH solution and calcined at different time intervals under temperatures of 100 and 200 °C. In Figures 1-a and 1-b, the diffractograms at 0 hours correspond to the post-synthesis, dried at 80°C. The XRD results obtained from the heat treatment of 100°C (Figure 1(a)) showed a diffraction parameter similar to the different calcination time intervals.

Figure 1. X-ray diffraction patterns. (a) ZnO nanoparticles (NaOH precipitating agent) calcined at 100°C in the range of 1 to 4 hours. (b) ZnO nanoparticles (NaOH precipitating agent) calcined at 200°C in the range of 1 to 4 hours. (c) Comparison of ZnO nanoparticles obtained by precipitation with NaOH and NH_4OH calcined at 200°C in 2 hours. The diffractograms at 0 hours are in the post-synthesis condition, dried at 80°C. The ZnO (Crysmet card no. 141145) and ZnO.nH_2O (Crysmet card no. 15008) patterns from the Crysmet database.

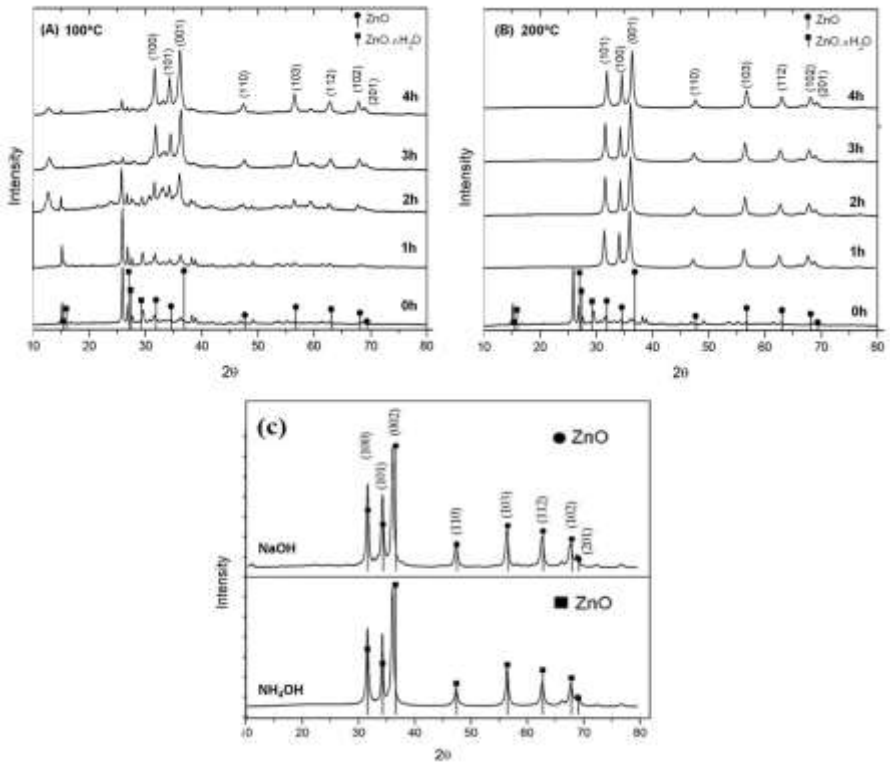

Source: Authors.

The diffraction peaks found at 2θ below 30° probably correspond to phases of the ZnO.nH_2O structures (Crysmet card no. 15008). The XRD of the samples calcined at 200°C (Figure 2(a)) present only diffraction peaks characteristic of ZnO with

the compact hexagonal wurtzite structure (Crysmet card no. 141145). With the increase in temperature from 100 to 200°C, the complete transformation of ZnO was obtained. The variation of calcination time showed that, after 2 hours at 200°C, the peak profile remains unchanged, with the formation of ZnO. Therefore, this synthesis condition is the best one according to the XRD data.

After establishing the best conditions for ZnO synthesis with NaOH as the precipitating agent, another synthesis was performed with NH_4OH instead of NaOH. The XRD data of ZnO nanoparticles with NH_4OH were compared to those with NaOH, as shown in Figure 1-c. Both diffractograms are similar.

Figure 2 shows the FESEM images of ZnO nanoparticles. This figure shows different morphologies such as wire, plate, and corn cob structures for the sample precipitated with NaOH and treated at 80°C (Figure 2-a). The nanostructures treated for 2 hours at 100°C show a predominance of phases with wire morphologies (Figure 2-b) and, at 200°C, wire and corn cob structures were found (Fig 2-c). The sample precipitated with NH_4OH (Figure 2-d), submitted to a heat treatment of 200°C for 2 hours, shows a spherical morphology evenly distributed.

Figure 2. FESEM micrographs of (a) ZnO nanoparticles (NaOH precipitating agent) at 0 hours in the post-synthesis condition, dried at 80°C (b) ZnO nanoparticles (NaOH precipitating agent) calcined at 100°C in 2 hours. (c) ZnO nanoparticles (NaOH precipitating agent) calcined at 200°C in 2 hours (d) ZnO nanoparticles obtained by the precipitation of NH_4OH calcined at 200°C in 2 hours. The feature shows morphology details.

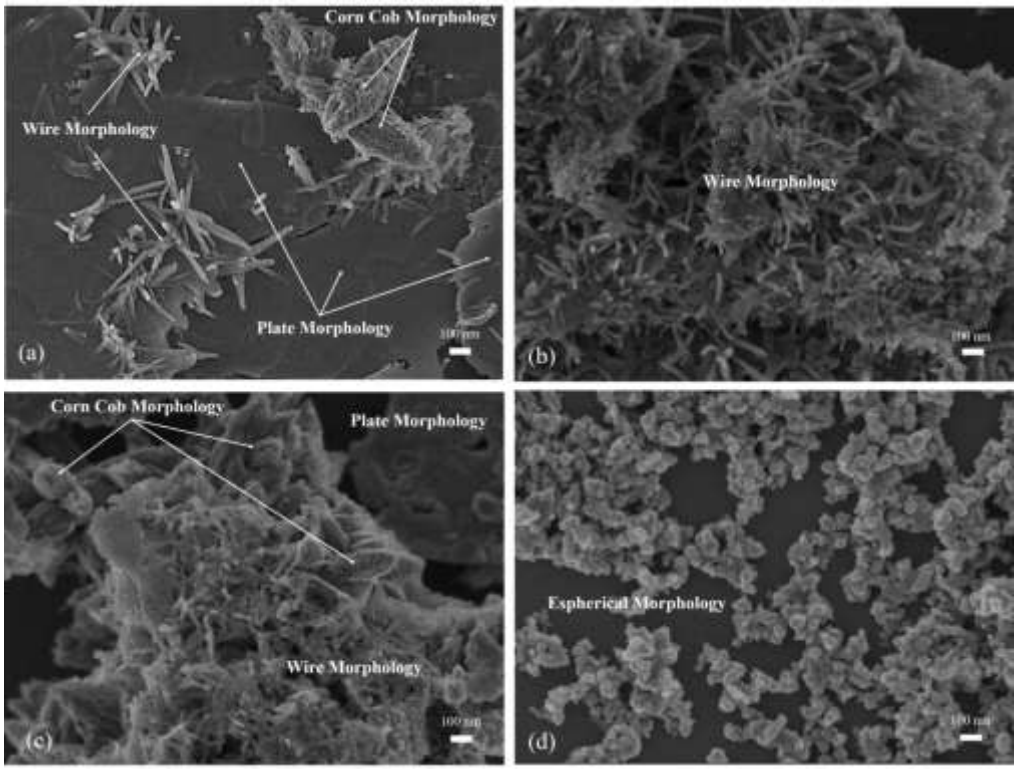

Source: Authors.

This may be linked to the influence of temperature and mainly to the precipitating agent, in which greater homogeneity and increased crystallinity are observed at higher temperatures, as shown in the X-ray diffractograms.

The FESEM images show the morphology variation according to the synthesis conditions. This result showed that the precipitating agent can change the size and shape of the nanomaterial and it is important for controlling the morphology and size of materials synthesized with the co-precipitation method. Liu et al. (2009) studied the NO_2 gas sensor based on ZnO

nanorods prepared with the hydrothermal method and, in this study, the authors found a decrease in the length of nanobar structures relative to temperature. The length values found were 1.78 μm (90°C), 1.43 μm (100°C), and 1.00 μm (110°C), while the nanorod diameter remained constant (30 nm) (Liu et al. 2009). Our study found the same behavior for nanobar lengths relative to temperature, measured in the SEM images. Considering the increased calcination temperature from 80 to 200°C, the average length was constant between 185 ± 70 nm(80°C) and 187 ± 63 nm (100°C) and the decrease in values for 124 ± 57 nm (200°C). The increase the diameters 29.4 ± 8.2 nm (80°C); 31.3 ± 13 nm (100°C); and 19.7 ± 12 nm (200°C), as shown in Fig 2 a-c. The average size of ZnO in Fig 2-d was 31.9 ± 12 nm.

Shi et al. (2013) evaluated the morphology of ZnO with wire structures, which can be controlled with a type of precursor, the molar ratio of reagents, and precipitating agents. The authors obtained ZnO nanoparticles with the method of alkaline hydrothermal synthesis at 335ºC using KOH and performed studies adding H_2O_2, suggesting different growth rates of ZnO crystals in the crystallographic plane under such conditions. The increased peroxide concentration significantly contributed to the growth of rods and a higher H_2O_2 ratio promoted edge sharpening and a rapid growth rate.

Montero-Muñoz et al. (2018) studied mechanisms of ZnO structure formation with the co-precipitation method, evidencing the controllable property of the morphology, and obtained different morphologies with direct precursor dependency using specific solvents and a single precipitating agent, as well as temperature variations of the heat treatment. In their study, three ZnO samples were synthesized with water, acetic acid, and ethylene glycol acidified with HNO_3 as solvents, which were all precipitated with NH_4OH. The results showed that ZnO obtained with water solvent and heat treatment at 300°C presented a needle/wire morphology, ZnO with acetic acid and heat treatment at 150°C showed a spherical morphology with clusters, and ZnO using ethylene glycol in an acidic medium showed a sponge morphology. This confirms the direct influence of such aspects on the variation of ZnO nanoparticle morphologies with the co-precipitation method.

The SEM images observed in Figure 2 show that precursors and calcination temperatures change the morphology and shape of ZnO nanoparticles. Adding a weak base makes nucleation the dominant stage while adding NaOH leads to the growth of wire and corn cob nanostructures as the dominant stage.

A change in morphology alters several properties of nanoparticles, such as colloidal stability. Figure 3 shows the zeta potential according to pH for nanostructures obtained at 200 °C (2 hours) precipitated with NaOH and NH_4OH. The zeta potential curves observed for the samples are similar, with potential values constantly negative and independent of pH. In these curves, the potentials become more negative as the pH increases, which indicates that this condition should be the most favorable for obtaining ZnO nanoparticles, with the best colloidal stability among the ZnO nanoparticles obtained.

Figure 3. Graph of zeta potential variation relative to pH for ZnO nanoparticles obtained at different calcination times: (a) 1 hour, (b) 2 hours, (c) 3 hours, and (d) 4 hours.

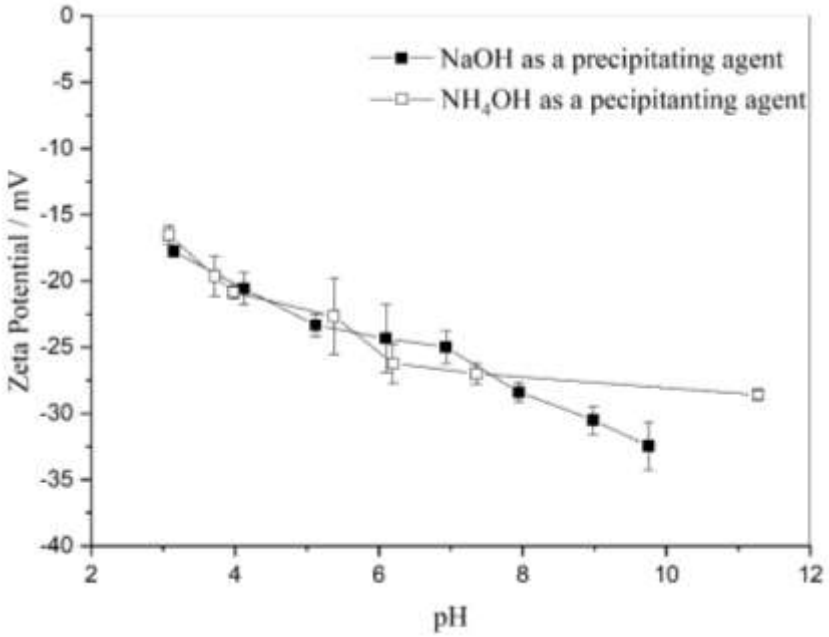

Source: Authors

Therefore, the results of X-rays, SEM, and zeta potential showed that the best crystallinity, morphology, and colloidal stability outcomes of ZnO nanoparticles are obtained at a calcination temperature of 200°C, for 2 hours, regardless of the precipitating agent.

The photocatalytic activity of ZnO nanostructures was studied by analyzing the degradation of the Rhodamine B (Rh B) dye. The degradation was monitored by studying the decrease in absorbance of the Rh B dye in the presence of ZnO suspensions. Figure 4 presents the UV/Vis spectra at different times for the study of rhodamine B (Rh B) degradation. The assays were performed with the *in natura* pH of the dye of around 6.5-7.0, at room temperature. The intensity of maximum absorbance at 554 nm of the dye decreased gradually over time, which indicated that the dye underwent a photocatalytic degradation by the ZnO nanostructure, as shown in Fig. 4-a and 4-b, respectively.

The results allow inferring that the concentration of Rh B decreases over time and degradation efficiency was higher with ZnO nanoparticles precipitated in NH_4OH medium (Figure 4(a)), presenting a complete removal of Rh B in an aqueous medium after 180 minutes of UV light exposure. When compared with the particles precipitated in NaOH medium for 180 minutes, the degradation was only 60-70% for the same time (Figure 4(b)), which indicates that the best material for the degradation of Rh B in the conditions studied was the ZnO nanoparticle precipitated with NH_4OH. The graph in Figure 5 shows this difference in degradation efficiency.

Figure 4. UV-Vis spectra obtained for the photodegradation of Rh B performed with catalysts: a) ZnO nanoparticles precipitated with NH_4OH and b) ZnO nanoparticles precipitated with NaOH.

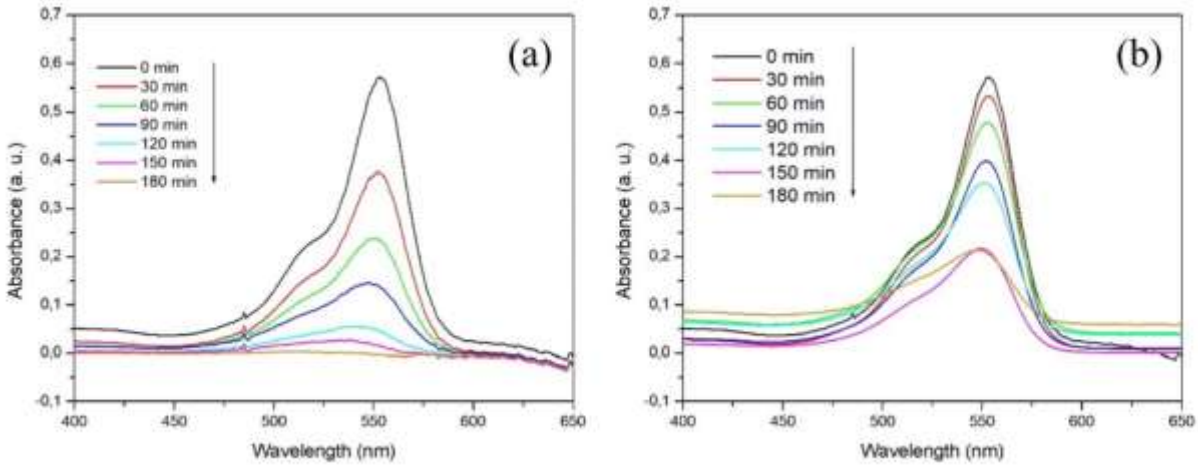

Source: Authors.

Figure 5. Graph of Rh B degradation efficiency using ZnO nanoparticles relative to time.

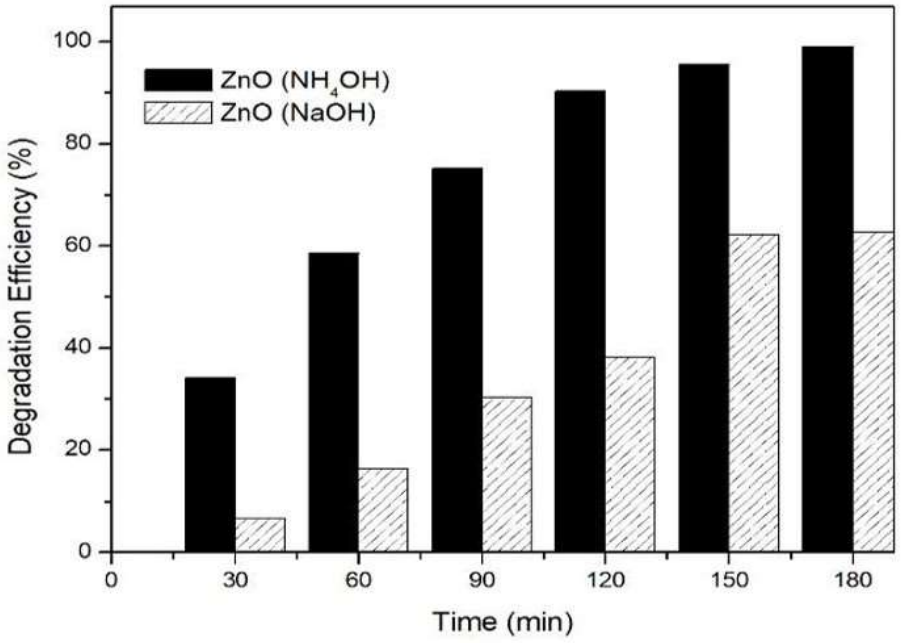

Source: Authors.

Graph 5 shows that degradation efficiency increases over time until around 180 minutes, which reached the rates of 100% and 67% of Rh B removal for ZnO precipitated with NH_4OH and NaOH, respectively. Therefore, it may be stated that the photocatalysts of ZnO precipitated with NH_4OH obtained a higher Rh B removal efficiency. Our results agree with Alvi et al. (2017), who synthesized ZnO in a solution with zinc nitrate hexahydrate, succinic acid, and sodium hydroxide, at 90°C for 8 hours. The material obtained was washed and dried at 50°C and presented a wire morphology, with variations of 80-100 nm. When applied to the process of Rh B photodegradation, a 97% degradation rate, after 120 minutes was obtained. Wang et al. (2015) and Gomes-solís et al. (2015) related high photocatalyst efficiency to the surface oxygen vacancies of the catalyst.

Wang et al. (2015) studied the surfactant effect resulting in different ZnO morphologies, such as nanoplates and small and rough particles, for the reaction of Rh B photodegradation. Their results evidenced the dependence of photocatalytic

activity on the morphology, showing that small particles with high concentrations of surface oxygen vacancy are the best catalysts for the reaction, combining structural and electrical effects, thus confirming photoactivity with the complete dye removal in one of the samples. They also indicated that the phenomenon of oxygen vacancy may accelerate the photocatalysis process because it can absorb species such as O_2^- and OH^-, showing an improved interaction between the catalyst and the organic pollutant. The ZnO nano-corn cob structures were studied by Gomes-Solís et al. (2015) and used in the process of methyl orange photodegradation in solar simulators, showing that synthesized structures are more efficient in this process than commercial ZnO, achieving 100% of dye degradation. The study also highlights that the photocatalytic activity of ZnO is attributed to polar and non-polar planes, as well as oxygen vacancies of the material. The study explained that, although the vacancies were linked to a narrowing of the band gap values compared to commercial ZnO, this phenomenon helped to prevent ZnO photocorrosion in solar simulators and increased catalyst efficiency in the process. This showed that the photocatalytic activity of a material depends on several factors that should be analyzed and correlated for good efficiency.

The band gap was calculated for the samples studied due to its direct relationship with efficiency in the photocatalysis process. Figure 6 shows the UV-Vis curves for the catalysts and highlights the $(\alpha h\upsilon)^2$ graph relative to energy, provided in eV. The band gap energy values, in eV, are provided by the line tangent to the inclination of curves graphically generated, resulting in the value in which the extension of this line intercepts axis x, corresponding to energy. These graphs show that the ZnO (NaOH) catalyst presents only one band in 371.9 nm and a band gap of 2.9 eV. The ZnO (NH_4OH) catalyst graph, in turn, presents two bands in 306 and 415 nm with band gap values of 2.7 and 3.2 eV, respectively.

Figure 6. UV-Vis spectra obtained for ZnO precipitated with (a) NaOH and (b) NH4OH. The graph of $(\alpha h\upsilon)^2$ relative to energy is highlighted in the figures.

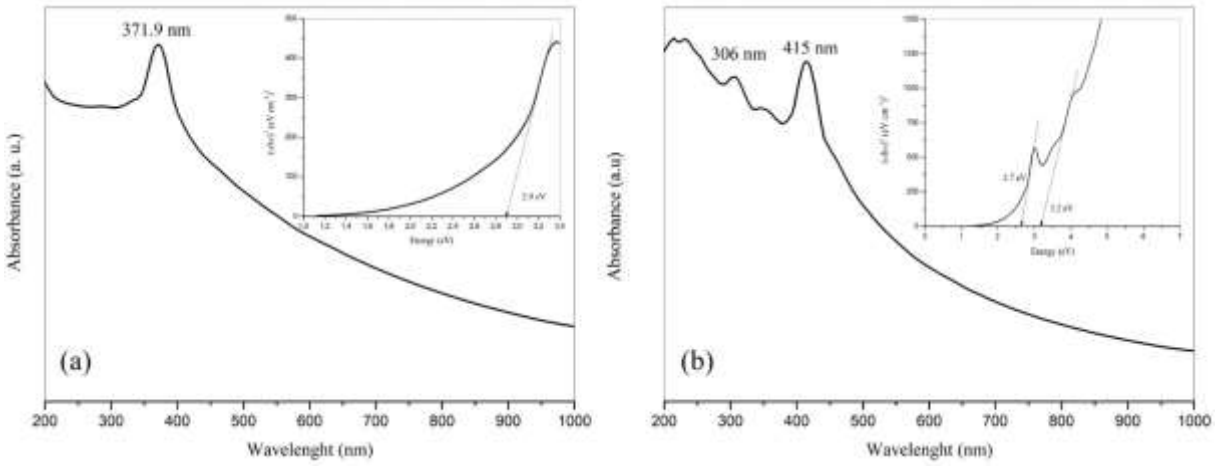

Source: Authors.

Rusdi et al. (2011) studied ZnO nanoparticles synthesized with the sol-gel method, obtaining different morphologies such as nanotubes, nanoroads, and spherical nanostructures, and correlated the direct influence of these morphologies on the band gap. The author proposed that, due to the strong internal interaction, the changed and reduced spacing in the ZnO network would affect the difference between the bands. Thus, the results indicated a value of 3.25 eV for the spherical morphology, 3.29 eV for nanoroads, and 3.35 eV for nanotubes, in which a smaller spacing in the crystalline structure showed higher band gap values. Montero-Muñoz et al. (2018) performed assays of photocatalytic decomposition of H_2O_2 in an aqueous solution with three ZnO samples with several variations of morphology, size, and band gap values. The samples were synthesized with different solvents and showed varying energy values of 3.16 eV, 3.18 eV, and 2.26 eV. The author correlated a study of the three variables of morphology, band gap, and degradation efficiency, verifying the direct influence of morphology on the

photodecomposition process. The study confirmed that wire/needle morphologies present crystalline defects that evidenced higher concentrations of oxygen and zinc vacancy in the interstice, located on the material surface, which stabilize the structure and work as active centers in the interface, as the morphology presented a band gap value of 3.16 eV and the best performance in the process studied.

Our results showed that zinc oxide nanoparticles with a wire/corn cob morphology precipitated with NaOH presented a value of 2.9 eV and the spherical morphology precipitated with NH_4OH showed values of 2.7 and 3.2 eV. The ZnO (NH_4OH) nanoparticles should present a higher density of electronic defects than ZnO (NaOH), producing energy levels between the band gaps. Hence, ZnO (NH_4OH) nanoparticles probably have another path to form the carriers of electron loads and holes, suggesting that this energy level would facilitate the production of reactive species on the surfaces. Therefore, a good photocatalytic performance involves variables that combine factors such as morphology, band gap, size, and surface area. The production of hydroxyl radicals associated with greater colloidal stability, morphology changes, and band gap for the comparison between two synthesized ZnO samples indicated an improved interaction between the dye and ZnO-NH_4OH, which was an excellent photocatalyst in the present study.

Tian et al. (2012) verified an excellent performance of ZnO as a catalyst for the degradation of methyl orange (MO), as well as an economical synthesis, using the solid phase method with zinc acetate dehydrated at 400, 600, 800, and 900°C. This represents an alternative to obtaining the material on a large scale with good efficiency and low cost, considering that a great portion of ZnO syntheses is based on the process of phase in solutions. The author explains the results of the influence of material temperature and crystallinity and consequently the different activities of microstructures on the photocatalytic process, showing that the combination of crystallinity and surface area are essential for an efficient process. Moreover, a 98% degradation rate is shown in 120 minutes for the ZnO-600 sample, with good reuse performance after five recycling processes. There is an important comparison between the processes of MO degradation with ZnO and another sample with TiO_2, which shows apparent degradation using ZnO about four times higher than the other catalyst. This shows that the activity of a photocatalyst is directly related to the morphology, crystalline structure, and surface area.

4. Conclusion

The synthesis of ZnO nanostructures shows a direct relationship between the different precipitating agents and morphology control over the nanomaterial studied, showing a wire/corn cob morphology for ZnO precipitated with NaOH and a spherical morphology for samples precipitated with NH_4OH. The X-ray diffractograms and SEM images showed a direct influence of the time interval of calcination and temperature on nanoparticle structures. The best synthetic conditions established were the temperature of 200°C and 2 hours for the heat treatment, showing a complete formation of the material. The synthesized ZnO nanoparticles were used as catalysts in the process of Rh B photodegradation. The ZnO precipitated with NaOH showed a percentage of 67% and ZnO precipitated with NH_4OH showed 100% of dye removal. Therefore, it is concluded that the good photocatalytic performance of the nanomaterial is linked to a combination of electronic, morphological, and superficial factors. The ZnO precipitated with NH_4OH presented the best photodegradation performance of organic compounds.

For suggestions for future work. One suggestion would be how the colloidal, photocatalytic and structural properties can be changed with the chemical modification of ZnO by other compounds.

Acknowledgments

This study was financed in part by the Coordenação de Aperfeiçoamento de Pessoal de Nível Superior – Brasil (CAPES) – Finance Code 001. The authors would like to thank the Brazilian agencies FAPESP and CNPq and acknowledge CEPID/CDMF – (FAPESP) grant No. 2013/07296-2.

References

Ahmad, S., Abbas, H., Khan, M. B., Nagal, V., Hafiz, A. K., & Khan, Z. H. (2021). ZnO for stable and efficient perovskite bulk heterojunction solar cell fabricated under ambient atmosphere. *Solar Energy*, 216, 164-170.

Alvi, M. A., Al-Ghamdi, A. A., & Shakeerakhtar, M. (2017). Synthesis of ZnO nanostructures via low temperature solution process for photocatalytic degradation of rhodamine B dye. *Materials Letter*, 204, 12-15.

Arya, S. K., Saha. S., Ramirez-Vick, J. R., Gupta, V., Bhansali, S., & Singh, S. P. (2012). Recent advances in ZnO nanostructures and thin films for biosensor applications: Review. *Analytica Chimicta Acta*, 737, 1-21.

Awan, F., Islam, M. S., Ma, Y., Yang, C., Shi, Z., Berry, R. M., & Tam, K. C. (2018). Cellulose Nanocrystal–ZnO Nanohybrids for Controlling Photocatalytic Activity and UV Protection in Cosmetic Formulation. *ACS Omega*, 3(10), 12403–12411.

Cavalcante, L.A., Aum, Y. K. P. G., Rebelo, Q.H.F., & Pocrifka, L. A. (2019). Evaluation of ZnO synthesized by pechini method in the degradation of blue methylene. *Brazilian Journal of Development*, 5(5), 3619-3626.

Cao, M., Wang, F., Zhu, J., Zhang, X., Qin, Y., & Wang, L. (2017). Shape-controlled synthesis of flower-like ZnO microstructures and their enhanced photocatalytic properties. *Materials Letters*, 192, 1-4.

Giraldi, T. R., Swerts, J. P., Vicente, M. A., De Mendonça, V. R., Paris, E. C., & Ribeiro, C. (2016). Utilização de partículas de ZnO: Mn para a degradação do azul de metileno por processo de fotocatálise. *Cerâmica*, 62, 345-350.

Gomez-Solís, C., Ballesteros, J. C., Torres-Martínez, L. M., Juárez-Ramírez, I., Díaz Torres, L. A., Zarazua-Morin, M. E., & Lee, S. W. (2015). Rapid synthesis of ZnO nano-corncobs from Nital solution and its application in the photodegradation of methyl orange. *Journal of Photochemistry and Photobiology* A, 298, 49–54.

Gu, X., Edvinsson, T., Zhu, J. (2020). ZnO nanomaterials: strategies for improvement of photocatalytic and photoelectrochemical activities. In: Wang X, Anpo M, & Fu X (Eds.), *Current Developments in Photocatalysis and Photocatalytic Materials* (p. 231-244). Oxford: Elsevier.

Jeong, W. J., Kim, S. K., & Park, G. C. (2006). Preparation and characteristic of ZnO thin film with high and low resistivity for an application of solar cell. *Thin Solid Films*, 506-507, 180–183.

Kouhail, M., Elberouhi, K., Elahmadi, Z., Benayada, A., & Gmouth, S. A. (2020). Comparative study between TiO2 and ZnO photocatalysis: Photocatalytic degradation of textile dye. IOP Conference Series: *Materials Science and Engineering*, 827, 012009.

Kumar, S., Dhiman, A., Sudhagar, P., & Krishnan, V. (2018). ZnO-graphene quantum dots heterojunctions for natural sunlight-driven photocatalytic environmental remediation. *Applied Surface Science*, 447, 802–815.

Kuo, C. L., Wang, C. L., Ko, H. H., Hwang, W. S., Chang, K., Li, W. L., & Wang, M. C. (2010). Synthesis of zinc oxide nanocrystalline powders for cosmetic applications. *Ceramics International*, 36(2), 693–698.

Lanje, A. S., Sharma, S.J., Ningthoujam, R.S., Ahn, J. S., & Pode, R. B. (2013). Low temperature dielectric studies of zinc oxide (ZnO) nanoparticles prepared by precipitation method. *Advanced Powder Technology*, 24(1), 331–335.

Liu, F. T., Gao, S. F., Pei, S. K., Tseng, S. C., & Liu, C. H. J. (2009). ZnO nanorod gas sensor for NO2 detection. *Journal of the Taiwan Institute of Chemical Engineers*, 40(5), 528–532.

Maia, G. A. R., Larsson, L. F. G., Viomar, A., Maia, E. C. R., De Santana, H., & Rodrigues, P. R. P. (2016). Aperfeiçoamento da produção de partículas de óxido de zinco para aplicação em células solares. *Cerâmica*, 62(361), 91-97.

Monteiro-Muñoz, M., Ramos-Ibarra, J. E., Rodrigues-Paez, J. E., Teodoro, M. D., Marques, G. E., Sanabria, A. R., & Coaquira, J. A. H. (2018). Role of defects on the enhancement of the photocatalytic response of ZnO nanostructures. *Applied Surface Science*, 448, 646–654.

Noreen, S., Khalid, U., Ibrahim, S. M., Javed, T., Ghani, A., Naz, S., & Iqbal, M. (2020). ZnO, MgO and FeO adsorption efficiencies for direct sky Blue dye: equilibrium, kinetics and thermodynamics studies. *Journal of Materials Research and Technology*, 9(3), 5881-5893.

Rusdi, R., Rahman, A. A., Mohamed, N. S., Kamarudin, N., & Kamarulzaman, N. (2011). Preparation and band gap energies of ZnO nanotubes, nanorods and spherical nanostructures. *Powder Technology*, 210(1), 18–22.

Salehi-Babarsad, F., Derikvand, E., Razaz, M., Yousefi, R., & Shirmardi, A. (2020). Heavy metal removal by using ZnO/organic and ZnO/inorganic nanocomposite heterostructures. *International Journal of Analytical Chemistry*, 100(6), 702-719.

Shetti, N. P., Bukkitgar, S. D., Reddy, K. R., Reddy, C. V., & Aminabhavi, T. M. (2019). ZnO-based nanostructured electrodes for electrochemical sensors and biosensors in biomedical applications. *Biosensors and Bioelectronics*, 141(15), 111417.

Shi, L., Naik, A. J. T., Goodall, J. B. M., Tighe, C., Gruar, R., Binions, R., & Darr, J. (2013). Highly Sensitive ZnO Nanorod- and Nanoprism-Based NO2 Gas Sensors: Size and Shape Control Using a Continuous Hydrothermal Pilot Plant. *Langmuir*, 29(33), 10603–10609.

Tian, C., Zhang, Q., Wu, A., Jiang, M., Liang, Z., Jiang, B., & Fu, H. (2012). Cost-effective large-scale synthesis of ZnO photocatalyst with excellent performance for dye photodegradation. *Chemical Communications*, 48(23), 2858-2860.

Walia, S., Weber, R., Balendhran, S., Yao, D., Abrahamson, J. T., Zhuiykov, S., & Kalantar-Zadeh, K. (2012). ZnO based thermopower wave sources. *Chemical Communications*, 48(60), 7462-7464.

Wang, L., Kang, Y., Liu, X., Zhang, S., Huang, W., & Wang, S. (2012). ZnO nanorod gas sensor for ethanol detection. *Sensors and Actuators B: Chemical*, 162, 237-243.

Wang, J., Yang, J., Li, X., Feng, B., Wei, B., Wang, D., & Song, H. (2015). Effect of surfactant on the morphology of ZnO nanopowders and their application for photodegradation of rhodamine. *Powder Technology*, 286, 269 -275.

Willander, M., Yang, L. L., Wadeasa, A., Ali, S. U., Asif, M. H., Zhao, Q. X., & Nur, O. (2019). Zinc oxidenanowires: controlled low temperature growth and some electrochemical and optical nano-devices. *Journal of Materials Chemistry*, 19(7), 1006–1018.

Zeng, P., Yu, H., Chen, M., Xiao, W., Li, Y., Liu, H., & Wang, X. (2020). Flower-like ZnO modified with BiOI nanoparticles as adsorption/catalytic bifunctional hosts for lithium-sulfur batteries. *Journal of Energy Chemistry*, 51, 21-29.